IMPACT OF LEAKAGE INLET SWIRL ANGLE IN A ROTOR-STATOR CAVITY ON FLOW PATTERN, RADIAL PRESSURE DISTRIBUTION AND FRICTIONAL TORQUE IN A WIDE CIRCUMFERENTIAL REYNOLDS NUMBER RANGE

T. R. Schröder, H.-J. Dohmen, D. Brillert, F.-K. Benra

Chair of Turbomachinery, University of Duisburg-Essen, Duisburg, Germany,
tilman.schroeder@uni-due.de

ABSTRACT

In side-chambers of radial turbomachinery, which form rotor-stator cavities, complex flow patterns develop that contribute substantially to axial thrust on the shaft as well as frictional torque on the rotor. Moreover, leakage flow through the side-chambers may occur in both centripetal as well as centrifugal direction, which significantly influences the rotor-stator cavity flow and has to be carefully considered in the design process: Precise correlations quantifying the effects of rotor-stator cavity flow are needed for the design of reliable and highly efficient turbomachines.

In this paper, centripetal leakage flow with and without pre-swirl in rotor-stator cavities is investigated experimentally, combining the experimental results from two test rigs: A hydraulic test rig covering the Reynolds number range $4 \cdot 10^5 \leq Re \leq 3 \cdot 10^6$ and a test rig for gaseous rotor-stator cavity flow which is operated at Reynolds numbers $2 \cdot 10^7 \leq Re \leq 2 \cdot 10^8$. These ranges cover the operating range of hydraulic as well as thermal turbomachinery. In rotor-stator cavities, Reynolds number Re is defined as $Re = \Omega b^2 \nu^{-1}$ with angular rotor velocity Ω, rotor outer radius b and kinematic viscosity ν. The influence of circumferential Reynolds number, axial gap width and centripetal through-flow on radial pressure distribution, axial thrust and frictional torque is presented, with through-flow being characterised by its mass flow rate and swirl angle at the inlet.

The results present a comprehensive insight into the flow in rotor-stator cavities with superposed centripetal through-flow and provide an extended database to aid the turbomachinery design process.

KEYWORDS

ROTOR-STATOR CAVITY, LEAKAGE FLOW, CENTRIPETAL THROUGH-FLOW

NOMENCLATURE

a	Hub radius
b	Disc radius
$\boldsymbol{b}$, $\boldsymbol{b}^*$	Column vector of Lagrange multipliers, used in curve fits
$c_D = \frac{\dot{m}}{\rho\, \Omega\, b^3}$	Mass flow coefficient
$c_F = \frac{2}{1-x_{\min}^2} \int_{x_{\min}}^{1} c_p(x)\, x \, \mathrm{d}x$	Axial thrust coefficient as function of c_p (large test rig)
$c_{Ff} = \frac{\pi b^2 p(r=b) - F_{af}}{\pi \Omega^2 b^4}$	Axial thrust coefficient in front cavity (small test rig)
$c_{Fb} = \frac{\pi [b^2 - a^2] p(r=b) - F_{af}}{\pi \Omega^2 [b^4 - a^4]}$	Axial thrust coefficient in back cavity (small test rig)

$c_L = \frac{\dot{m}^2 \tan\alpha}{4\pi^2\rho^2 b^5 \Omega^2 d}$	Through-flow angular momentum coefficient
$c_{Ms} = \frac{2M}{\rho\, \Omega^2\, b^5}$	Torque coefficient for one disc side
$c_p(x) = \frac{p(x=1)-p(x)}{\rho\Omega^2 b^2}$	Pressure coefficient
d	Width of centripetal through-flow inlet gap
F_a, F_{ab}, F_{af}	Axial thrust, axial thrust in back and front cavity
$G = \frac{s}{b}$	Relative axial gap width
i, j	Indices of matrix components
$K = \frac{v_\varphi}{\Omega r}$	Core swirl factor
$\dot{m}$	Mass flow rate of through-flow
$\boldsymbol{M}(\boldsymbol{x}, \boldsymbol{y})$, $\boldsymbol{M}^*(\boldsymbol{x}, \boldsymbol{w})$	Column vector of model functions/extended model functions
$p(x)$	Pressure at relative radial position x
$p_b(r)$, $p_f(r)$	Pressure at radial position r in back and front cavity, respectively
$\boldsymbol{Q}$	Sensitivity matrix, used in curve fit error propagation
r	Radial position
$Re = \frac{\Omega b^2}{\nu}$, $Re_r = x^2 Re$	Circumferential Reynolds number, local Reynolds number
s, s_{back}	Axial gap width, axial gap width of back cavity
T_{all}, T_{friction}	Overall torque, frictional torque of bearings and fluid friction
$\boldsymbol{U}_{xx}$, $\boldsymbol{U}_{w^*w^*}$, u	Matrices of covariances, covariance component
v_φ	Circumferential fluid velocity
$\boldsymbol{w} = (\boldsymbol{b}^T, \boldsymbol{y}^T, \boldsymbol{z}^T)^T$, $\boldsymbol{w}^*$	Column vector of all unknown values, used in curve fits
$x = \frac{r}{b}$	Relative radial position
$x_{\min} = \frac{r_{\min}}{b}$	Minimal relative radial pressure measurement position
$\boldsymbol{x} = (x_1, \ldots, x_n)^T$	Column vector of measured values, used in curve fits
$\boldsymbol{y} = (y_1, \ldots, y_m)^T$, $\boldsymbol{y}^*$	Column vector of model parameters, used in curve fits
$\boldsymbol{z} = (z_1, \ldots, z_n)^T$, $\boldsymbol{z}^*$	Column vector of fitted values, replaces $\boldsymbol{x}$ in model function
α	Swirl angle ($\alpha = 0$ no swirl, $\alpha > 0$ corotating swirl)
ν	Kinematic viscosity
ρ	Density
χ^2	Least squares function, used in curve fits
Ω	Angular velocity of the rotor
$\mathcal{L}$	Lagrange function

INTRODUCTION

In rotor-stator cavities, which are found in all radial turbomachines, complex flow patterns occur and influence axial thrust on the shaft as well as disc-friction torque. For a reliable design of axial bearings, maximum axial thrust on the shaft must be known with sufficient precision during the design phase of a radial turbomachine. Moreover, for high efficiency, losses due to friction in the cavities should be minimal, which can be achieved by a careful design of cavity geometry.

The first thorough experimental study of turbulent rotor-stator cavity flow was performed by Daily and Nece (1960), with their test rig able to reach Reynolds numbers up to $Re = 10^7$. Based on their torque measurements they identified two turbulent flow regimes, where rotor and stator boundary layers are either merged or separated. In the case of separated boundary layers, their velocity measurements indicate the existence of a fluid core in the cavity middle, where radial velocity is negligible and circumferential velocity varies only with radius, not with axial coordinate. The existence of these regimes depend on circumferential Reynolds number Re and relative axial gap width G. They introduced empirical correlations for torque coefficient c_{Ms} for each flow regime.

In Kurokawa and Toyokura (1972) and Kurokawa and Sakuma (1988) models for rotor-stator cavity flow with through-flow are introduced, which are based on assumed velocity profiles as well as wall shear stress measurements. The models allow for the calculation of radial pressure distribution and axial thrust for the cases of closed cavity and centripetal through-flow. Moreover, they take into account the angular momentum flux into the cavity in the through-flow case.

Radtke and Ziemann (1982) experimentally investigated not only closed rotor-stator cavities, but also centripetal and centrifugal through-flow with and without preswirl as well as variations of the cavity geometry. Their results give a detailed outline of the influences of the variations investigated.

Poncet et al. (2005a) investigate turbulent flow in a rotor-stator cavity with centripetal through-flow in the Reynolds number range $1.04 \cdot 10^6 \leq Re \leq 4.2 \cdot 10^6$ at relative cavity widths $0.024 \leq G \leq 0.048$. They show experimental results at through-flow mass flow coefficients $2.5 \cdot 10^{-3} \leq c_D \leq 10^{-2}$ and report validity of their theoretical model in an even wider range of Reynolds number and through-flow mass flow coefficients. In their paper, LDA measurements of core swirl ratio $K(v_\varphi)$ are compared to predictions of core swirl ratio $K(p(r))$ based on measurements of radial pressure distribution $p(r)$. The theoretical model is a $5/7$ power law relating core swirl ratio K, local Reynolds number $Re_r = x^2 Re$ and through-flow mass flow coefficient c_D.

Poncet et al. (2005b) propose a new Reynolds stress turbulence model suitable for numerical investigations of rotor-stator cavity flow that is reported to be superior to k-ε turbulence models for this application. They investigate mean flow structure, core swirl ratio K, radial pressure distribution and turbulence statistics for closed cavities, and centripetal as well as centrifugal through-flow. This publication gives a comprehensive summary of flow structures with separated boundary layers inside rotor-stator cavities.

Will (2011) investigates centripetal as well as centrifugal flow in a rotor-stator cavity, using analytical, experimental and numerical methods. He develops a new one-dimensional flow model of core swirl ratio K, assuming separated boundary layers and using the logarithmic law of the wall.

Wang et al. (2018) performed PIV measurements in a water-filled microscale rotor-stator cavity made of glass with smooth and hydrophobic discs at low Reynolds numbers. They found a reduction of torque coefficient c_{Ms} of more than 50% when using hydrophobic rotors, which was attributed to a thin air layer between disc and liquid in the case of hydrophobic rotor surfaces as well as a reduction of turbulence intensities.

In the present study, experimental results of two rotor-stator test rigs are combined: The small test rig is operated with water, may be equipped with different discs with outer radius $b = 110\text{mm}$ each and is made of PMMA (Plexiglass). It covers the range of Reynolds numbers $3.8 \cdot 10^5 \leq Re \leq 3.2 \cdot 10^6$ and the axial gap width range $0.0182 \leq G \leq 0.0728$. A more detailed description can be found in Hu et al (2017a, 2017b) and Hu (2018). The large test rig, first introduced by Barabas et al. (2015), can reach Reynolds numbers up to $Re = 2.5 \cdot 10^8$ due to its large disc radius of $b = 400\text{mm}$ and its operation with carbon dioxide. Relative gap widths of $0.0125 \leq G \leq 0.0375$ are investigated in this test rig. Both rigs allow the superimposition of centripetal through-flow with different inlet swirl angles, leading to through-flow rate coefficients $-6.64 \cdot 10^{-3} \leq c_D \leq 0$ for the small and $-1.45 \cdot 10^{-3} \leq c_D \leq 0$ for the large test rig, respectively. Negative coefficients c_D mean centripetal through-flow. Concerning angular momentum inflow at the centripetal inlet, the small test rig covers the range $0 \leq c_L \leq 9.6 \cdot 10^{-5}$ and the large one $0 \leq c_L \leq 1.6 \cdot 10^{-5}$, positive c_L values denoting corotating swirl.

ROTOR STATOR CAVITY TEST RIGS, MEASUREMENT PROCEDURES AND UNCERTAINTY CALCULATION

A schematic of the Rotor-stator test rigs that have been used in this study can be seen in Figure 1. The rotor has angular velocity Ω, outer radius b, and hub radius a. Cavity width is given by distance s. Through-flow with mass flow rate $\dot{m}$ enters the cavity through the centripetal swirl generator, which has inlet width d, and exits axially at the hub. In the case of a closed cavity, centripetal swirl

generators are replaced by a ring structure, resulting in a cylindrical shroud without any opening. The small test rig does not have a hub in its front cavity according to Hu (2018).

Axial thrust measurement technique in the small test rig is described in detail in Hu (2018) and summarised here. In the small test rig, tension-compression force transducers and a linear ball bearing are used to measure axial thrust on rotor and shaft. Sum of axial forces on both parts reads

$$F_a = F_{ab} - F_{af} = \int_{A_b} p_b(r)\mathrm{d}A - \int_{A_f} p_f(r)\mathrm{d}A = -\pi a^2 p(b) - \pi\Omega^2\rho\left[c_{Fb}[b^4 - a^4] - c_{Ff}b^4\right] \quad (1)$$

where F_a is the axial force measured by tension-compression force transducers, and F_{ab} and F_{af} are axial force due to pressure in back and front cavity, respectively. Radial pressure distribution in back and front cavity is characterised by axial thrust coefficients c_{Fb} and c_{Ff}, respectively. In the case of closed cavity without through-flow and $s = s_{\text{back}}$, equal flow structures in front and back cavity are assumed, which leads to the assumption $c_{Fb} = c_{Ff}$. From measurements of net axial thrust F_a in this test rig configuration a correlation for c_{Fb} is calculated, which is then used to calculate axial thrust coefficients c_{Ff} from net axial force (F_a) measurements in different test rig configurations.

The large test rig has nine pressure taps to measure radial pressure distribution, where differential pressure transducers are installed to measure pressure differences $p(b) - p(x)$ directly. Furthermore, temperature and absolute pressure are measured at outer radius b. From these measurements, density ρ and kinematic viscosity ν are calculated. Integrals in axial thrust coefficients c_F are approximated using the trapezoidal rule.

Calculation of torque coefficients c_{Ms} is done in both test rigs (compare Hu (2018)) as follows: Overall torque T_{all} is measured between motor and coupling, and includes friction torque T_{friction} generated by bearings and fluid friction on shaft. Fluid friction in the back cavity is modelled by a correlation, $c_{Ms,\,\text{back}}$, and friction on the cylindrical outer rotor surface is given by a correlation $c_{Ms,\,\text{cylindrical}}$. This leads to

$$c_{Ms} = \frac{2[T_{\text{all}} - T_{\text{friction}}(p,\Omega)]}{\rho\Omega^2 b^5} - c_{Ms,\,\text{back}} - c_{Ms,\,\text{cylindrical}} \quad (2)$$

where $T_{\text{friction}}(p,\Omega)$ is a correlation derived from measurements with no disc installed. In the large test rig, this is conducted at different CO_2 pressure levels p and the shaft rotating at varying angular velocities Ω, in the small test rig only angular velocity Ω is varied according to Hu (2018).

The correlation $c_{Ms,\,\text{back}}$ was found by setting equal front and back cavity widths ($s = s_{\text{back}}$) with the test rigs in closed cavity configuration, and assuming $c_{Ms,\,\text{front}} = c_{Ms,\,\text{back}}$. Overall torque T_{all} at varying angular velocity Ω (and pressure p in the large test rig) was measured, then $c_{Ms,\,\text{back}}$ was found from

$$2c_{Ms,\,\text{back}} = \frac{2[T_{\text{all}} - T_{\text{friction}}(p,\Omega)]}{\rho\Omega^2 b^5} - c_{Ms,\,\text{cylindrical}} \quad (3)$$

Radtke and Ziemann (1982) published a correlation $c_{Ms,\text{cylindrical}}$ for friction on cylindrical outer rotor surfaces in rotor-stator cavities. It is assumed that this correlation holds for friction on this surface in both test rigs, although extrapolation to larger Reynolds numbers than investigated by Radtke and Ziemann (1982) is needed in the large test rig case. According to Hu (2018), $c_{Ms,\,\text{cylindrical}}$ is neglected in the small test rig.

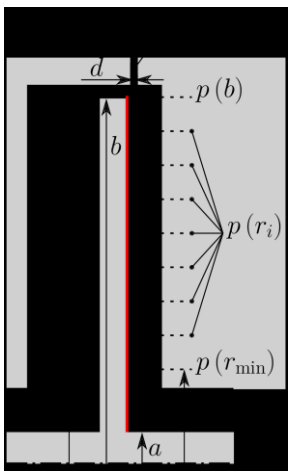

Figure 1: Schematic of the Rotor-stator cavity test rigs used. Dashed lines indicate pressure measurements, torque coefficients c_{Ms} correspond to the torque acting on the surface indicated by the red line. The small test rig does not have a hub in its front cavity according to Hu (2018).

Calculation of torque coefficients c_{Ms} uncertainties of the large test rig include torque transducer measurement uncertainty, breakaway torque, fluid density uncertainty resulting from temperature and absolute pressure

measurement uncertainty, angular velocity measurement uncertainty and manufacturing tolerances. Uncertainty of the correlation $c_{Ms,\,\mathrm{cylindrical}}$ is not known and not included in the calculation, meaning that torque coefficient uncertainties are a lower bound. To calculate uncertainties, first order error propagation is used as presented in Bevington and Robinson (2003). Uncertainties of measurements in the small test rig are taken from Hu (2018).

Calculation of curve fits and model parameter uncertainties is carried out as presented in Weise and Wöger (1999), and is briefly summarised here. Let $\boldsymbol{x} = (x_1, \ldots, x_n)^T$ be a column vector of measured values with associated covariances $u(x_i, x_j)$ and $\boldsymbol{y} = (y_1, \ldots, y_m)^T$ be a column vector of unknown model parameters. The column vector of model equations is given by $\boldsymbol{M}(\boldsymbol{x}, \boldsymbol{y}) = 0$. Measured values $\boldsymbol{x}$ will most likely not fulfil the model $\boldsymbol{M}(\boldsymbol{x}, \boldsymbol{y}) = 0$ for any vector of model parameters $\boldsymbol{y}$, therefore $\boldsymbol{x}$ is replaced by a column vector $\boldsymbol{z} = (z_1, \ldots, z_n)^T$ of free parameters that should fulfil $\boldsymbol{M}(\boldsymbol{z}, \boldsymbol{y}) = 0$ while minimising the squared error norm χ^2. This error norm assigns a high weight to measurement results with low uncertainties and vice versa. This problem is solved, using a column vector $\boldsymbol{b}$ of Lagrange multipliers, for the unknown column vector $\boldsymbol{w} = (\boldsymbol{b}^T, \boldsymbol{y}^T, \boldsymbol{z}^T)^T$ by finding a Karush-Kuhn-Tucker point $\boldsymbol{w}^*$ of the Lagrange function

$$\mathcal{L}(\boldsymbol{x}, \boldsymbol{w}) = \frac{1}{2}\chi^2 + \boldsymbol{M}^T(\boldsymbol{z}, \boldsymbol{y}) \cdot \boldsymbol{b} = \frac{1}{2}[\boldsymbol{z} - \boldsymbol{x}]^T \cdot \boldsymbol{U}_{xx}^{-1} \cdot [\boldsymbol{z} - \boldsymbol{x}] + \boldsymbol{M}^T(\boldsymbol{z}, \boldsymbol{y}) \cdot \boldsymbol{b}. \qquad (4)$$

Here, $(U_{xx})_{ij} = u(x_i, x_j)$ are components of the matrix $\boldsymbol{U}_{xx}$ of measurement covariances. The Karush-Kuhn-Tucker conditions for this problem, which are solved for $\boldsymbol{w}$, read

$$\boldsymbol{M}^*(\boldsymbol{x}, \boldsymbol{w}) = \begin{pmatrix} \nabla_{\boldsymbol{b}} L(\boldsymbol{x}, \boldsymbol{w}) \\ \nabla_{\boldsymbol{y}} L(\boldsymbol{x}, \boldsymbol{w}) \\ \nabla_{\boldsymbol{z}} L(\boldsymbol{x}, \boldsymbol{w}) \end{pmatrix} = \begin{pmatrix} \boldsymbol{M}(\boldsymbol{z}, \boldsymbol{y}) \\ \dfrac{\partial \boldsymbol{M}^T(\boldsymbol{z}, \boldsymbol{y})}{\partial \boldsymbol{y}} \cdot \boldsymbol{b} \\ \boldsymbol{z} - \boldsymbol{x} + \boldsymbol{U}_{xx} \cdot \dfrac{\partial \boldsymbol{M}^T(\boldsymbol{z}, \boldsymbol{y})}{\partial \boldsymbol{z}} \cdot \boldsymbol{b} \end{pmatrix} = 0. \qquad (5)$$

A solution $\boldsymbol{w}^* = \left(\boldsymbol{b}^{*T}, \boldsymbol{y}^{*T}, \boldsymbol{z}^{*T}\right)^T$ to these conditions includes the vector $\boldsymbol{y}^*$ of optimal model parameters.

Covariances $u(w_i^*, w_j^*)$, including covariances $u(y_i^*, y_j^*)$ of optimal model parameters $\boldsymbol{y}^*$, are derived by first order error propagation and are given by

$$\boldsymbol{U}_{w^*w^*} = \boldsymbol{Q}(\boldsymbol{w} = \boldsymbol{w}^*) \cdot \boldsymbol{U}_{xx} \cdot \boldsymbol{Q}^T(\boldsymbol{w} = \boldsymbol{w}^*) \qquad (6)$$

$$\boldsymbol{Q}(\boldsymbol{w}) = -\left[\frac{\partial \boldsymbol{M}^*(\boldsymbol{x}, \boldsymbol{w})}{\partial \boldsymbol{w}}\right]^{-1} \cdot \frac{\partial \boldsymbol{M}^*(\boldsymbol{x}, \boldsymbol{w})}{\partial \boldsymbol{x}} \qquad (7)$$

Here, $(\boldsymbol{U}_{w^*w^*})_{ij} = u(w_i^*, w_j^*)$ are the components of the matrix $\boldsymbol{U}_{w^*w^*}$ of covariances of the vector $\boldsymbol{w}^*$. Standard uncertainties $u(y_i^*)$ are then given by $u(y_i^*) = \sqrt{u(y_i^*, y_i^*)}$.

If uncertainties of measured values are unknown, the curve fit method reduces to finding $\boldsymbol{y}^*$ that minimises $\frac{1}{2}\boldsymbol{M}^T(\boldsymbol{x}, \boldsymbol{y}^*) \cdot \boldsymbol{M}(\boldsymbol{x}, \boldsymbol{y}^*)$.

CLOSED CAVITY

The flow in a closed cavity, which has no preswirl guide vanes installed and has a cylindrical shroud, is taken as the reference configuration. This is the configuration originally investigated by Daily and Nece (1960). In this section, the dependency of torque coefficient c_{Ms}, radial pressure distribution cofficient c_p and axial thrust coefficient c_F on circumferential Reynolds number Re_φ and relative axial gap width G is investigated. In later sections, the influence of centripetal through-flow is compared to this reference configuration.

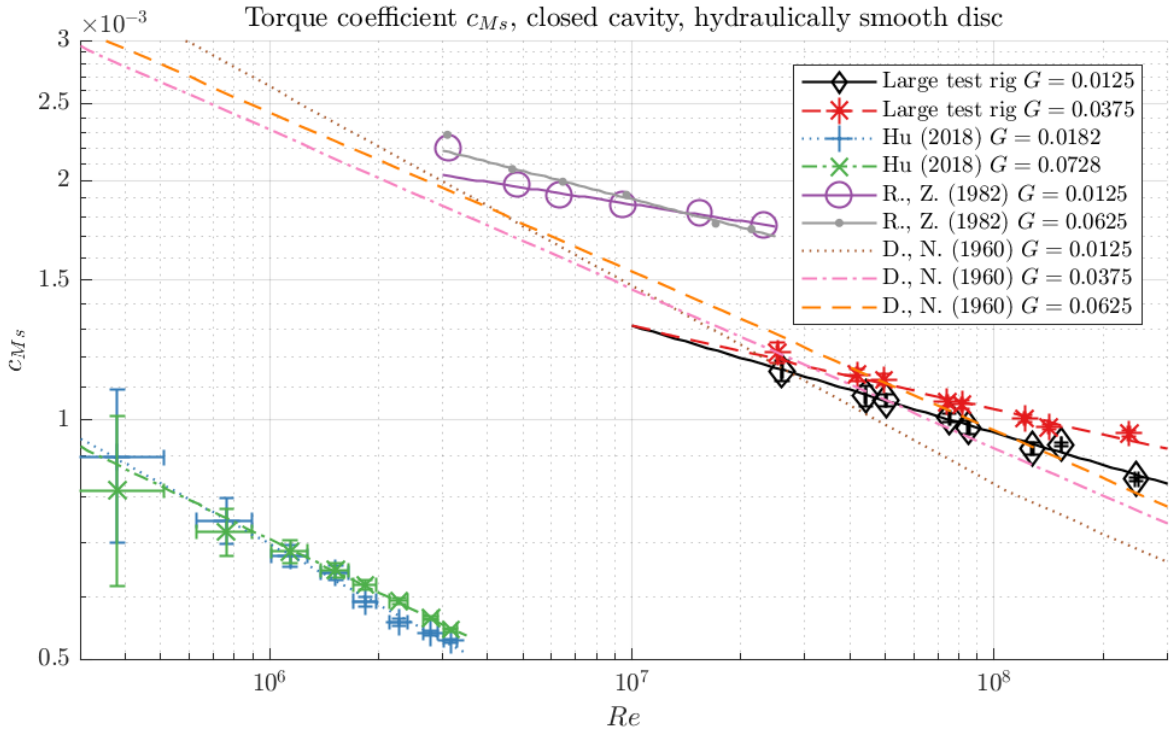

Figure 2: Torque coefficient of a closed rotor-stator cavity with hydraulically smooth disc. Lines belonging to measurement points are curve fits. "R., Z. (1982)" refers to Radtke and Ziemann (1982), "D., N. (1960)" refers to Daily and Nece (1960).

Torque coefficient

In the design process of radial turbomachinery, frictional losses in side chambers should be minimised. The gap width has a significant influence on frictional losses; the correlations by Daily and Nece (1960) showed that the minimal torque is found in the transition zone between the two flow regimes. Moreover, they found that for merged and separated boundary layers, the torque coefficient c_{Ms} is proportional to $Re^{-0.25}$ and $Re^{-0.20}$, respectively.

In Figure 2, torque measurements of closed cavities with hydraulically smooth discs are shown: This figure compares data from the small, water operated test rig, the large carbon dioxide test rig, the test bench used in Radtke and Ziemann (1982) and the correlations by Daily and Nece (1960). All uncertainties shown in this paper are 99% confidence levels (2.576σ), all quoted in text are one standard deviation uncertainties.

The low torque coefficient values of the small test rig are a result of the hydrophobic properties of the material used and its low surface roughness: PMMA is used for both the disc and the casing, its transparency meaning that its surface is very smooth. In the large, carbon dioxide operated test rig, the disc used is polished and hydraulically smooth at all Reynolds numbers investigated. Optical roughness measurements of disc surface do not show any significant surface roughness. In contrast, shroud and casing are rough, the casing roughness being approximately 10µm tip-to-tip. Moreover, holes are drilled in the cylindrical outer disc surface for balancing, which increases measured torque. For these reasons, only variations of torque coefficient c_{Ms} with Reynolds number Re and relative axial gap width G are investigated for the closed cavity. With torque resulting from bearing friction, fluid friction on the shaft, friction on the disc backside and friction on the cylindrical outer disc surface subtracted, the torque coefficient c_{Ms} indicates only friction torque on the disc front side.

For the small test rig, development of torque coefficient c_{Ms} with increasing Reynolds number Re shows a good agreement with the results of Daily and Nece (1960), with torque coefficients c_{Ms} being proportional to $Re^{-0.253\pm0.01}$ and $Re^{-0.223\pm0.009}$ for the small cavity width $G = 0.0182$ and the large cavity width $G = 0.0728$, respectively. In this range up to $Re = 4 \cdot 10^6$ and with incompressible fluids, no deviation from the predictions made by Daily and Nece (1960) can be

recognised. Measurements at small cavity width $G = 0.0182$ are in the merged boundary layer regime, while all measurements at large cavity width $G = 0.0728$ feature separated boundary layers according to Daily and Nece (1960).

The large test rig and the test bench used in Radtke and Ziemann (1982) are operated with compressible gases, carbon dioxide and air, respectively. Furthermore, they operate in Reynolds number regions $Re \geq 3 \cdot 10^6$. Torque data from these test rigs shows that with increasing Reynolds number Re, torque coefficient c_{Ms} decreases significantly slower than in the range $Re \leq 4 \cdot 10^6$: The largest torque coefficient decrease is proportional to $Re^{-0.134 \pm 0.003}$ (large test rig, $G = 0.0125$), the slowest is proportional to $Re^{-0.07}$ (Radtke and Ziemann (1982), $G = 0.0125$). This shows that regimes introduced by Daily and Nece (1960) cannot reliably be applied to rotor-stator cavities at Reynolds numbers $Re \geq 10^7$. It is important to note that both test rigs show a different behaviour of torque coefficient c_{Ms} with respect to the relative cavity width G: The data by Radtke and Ziemann (1982) show that with increasing relative cavity width G, the exponent c in $c_{Ms} \propto Re^c$ decreases, while the data from the large test rig shows the opposite: The exponent increases with increasing relative cavity width G.

Radial pressure distribution

A radial pressure gradient develops in rotor-stator cavities, which is a source of axial thrust on the rotor disc or on the shaft in a radial turbomachine. For a precise prediction of axial thrust, the radial pressure distribution must be known for the operating point of the machine.

Kurokawa and Sakuma (1988) proposed two models to calculate the core swirl ratio K (with circumferential velocity v_φ at cavity middle $z = s/2$) and the radial pressure distribution coefficient c_p for rotor-stator cavities without through-flow as well as centripetal through-flow. The models are called interference and non-interference gap models, because they are based on characteristics of two flow regimes identified by Daily and Nece (1960): The interference gap model assumes the absence of a rotating core, rotor and stator boundary layers with a thickness of half cavity width each, and velocity distributions according to the $1/7$ power law. For the non-interference gap model, a rotating

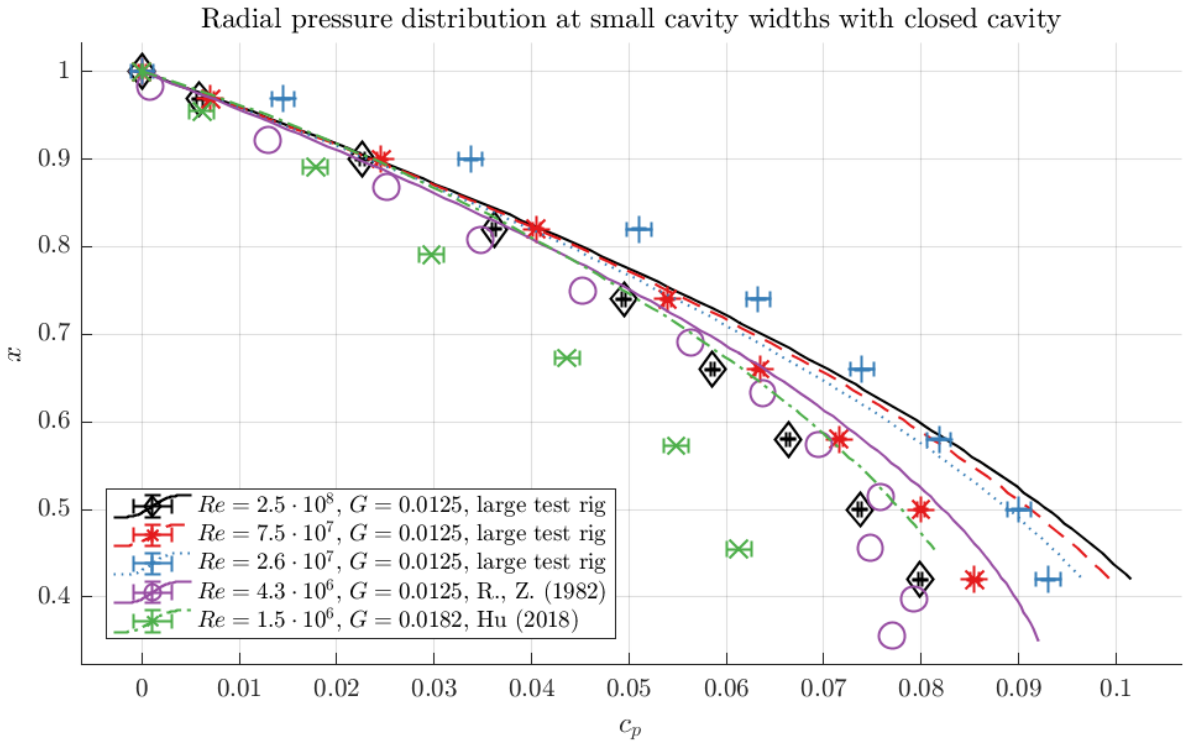

Figure 3: Radial pressure distribution at small cavity widths with closed cavity. Markers denote measurements; lines are predictions from the models proposed by Kurokawa and Sakuma (1988).

core with axially constant circumferential velocity and vanishing radial velocity is assumed to exist between the boundary layers. The models take into account the circumferential Reynolds number Re and the relative cavity width G.

In Figure 3, variation of radial pressure distribution for a range of circumferential Reynolds numbers at a small cavity width is shown. Measurement data of the small test rig is taken from Hu (2018). Markers denote measurements; lines are predictions from the models proposed by Kurokawa and Sakuma (1988). According to Kurokawa and Sakuma (1988), only the small test rig operates in the non-interference gap region, all other measurements are at operating conditions with interfering boundary layers. Measurements in Reynolds number range $1.5 \cdot 10^6 \leq Re \leq 2.6 \cdot 10^7$ show that with increasing Reynolds number Re, radial pressure gradient increases, and at $Re \approx 2.6 \cdot 10^7$ radial pressure gradient is largest. Although the models by Kurokawa and Sakuma (1988) fail to predict pressure coefficients c_p precisely, they capture this increase of radial pressure gradient with increasing Reynolds number Re. A further increase of Reynolds number Re to the range $Re \geq 3 \cdot 10^7$ leads to a decrease of radial pressure gradient, while the models by Kurokawa and Sakuma (1988) predict a further increase. In the small test rig, the changes of radial pressure gradient with Reynolds number are small for the relative cavity width $G = 0.0182$, so only one representative set of measurements is shown.

Axial thrust coefficient

In Figure 4, axial thrust coefficients c_F derived from measurements are plotted versus Reynolds number Re for different relative cavity widths G for both test rigs. With increasing Reynolds number Re, axial thrust coefficient c_F decreases, while the increase of cavity width results in a decrease of axial thrust coefficient c_F. For the small test rig, axial thrust coefficient c_F decreases significantly faster with increasing Reynolds number Re than for the large test rig. Moreover, with the small relative cavity width $G = 0.0182$, decrease of axial thrust coefficient c_F slows down for Reynolds numbers $Re \geq 2 \cdot 10^6$, so its slope in this range is much closer to the slope of axial thrust coefficients obtained from the large test rig. There seems to be a change in flow characteristics generating this change in slope, for example increasing influence of turbulence. Further research is needed to investigate this phenomenon. Data from small and large test rig show a continuous decline of axial thrust coefficients c_F, there is no hint of discontinuities or other phenomena in the Reynolds number range where no measurement data is available.

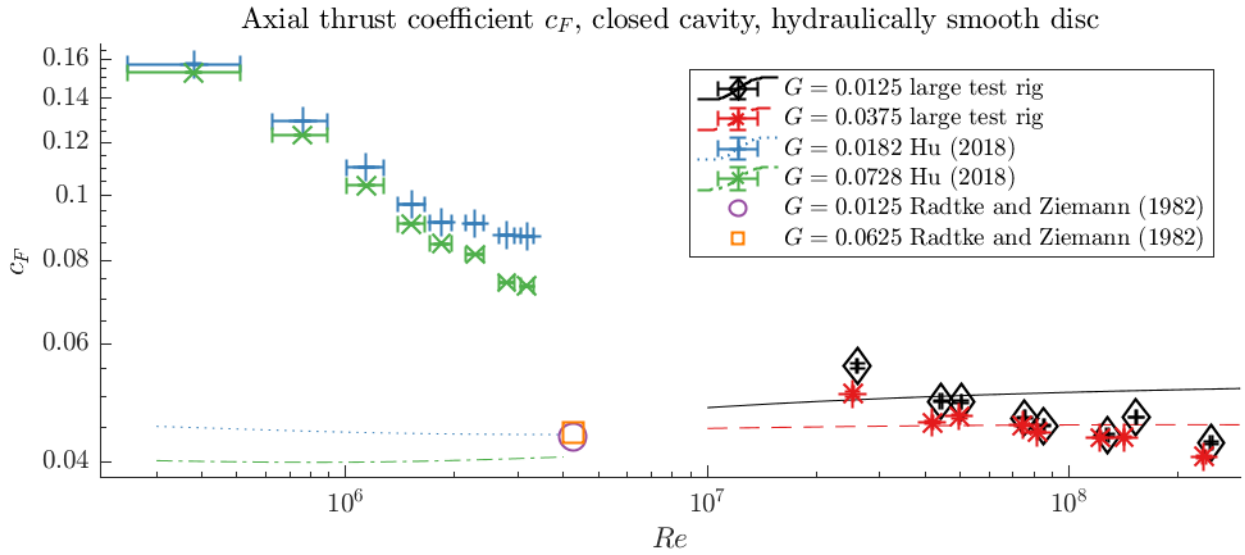

Figure 4: Axial thrust coefficient of small and large test rig as well as from Radtke, Ziemann (1982). Markers are measurements; lines show the corresponding prediction from the models by Kurokawa and Sakuma (1988). Small test rig data is taken from Hu (2018).

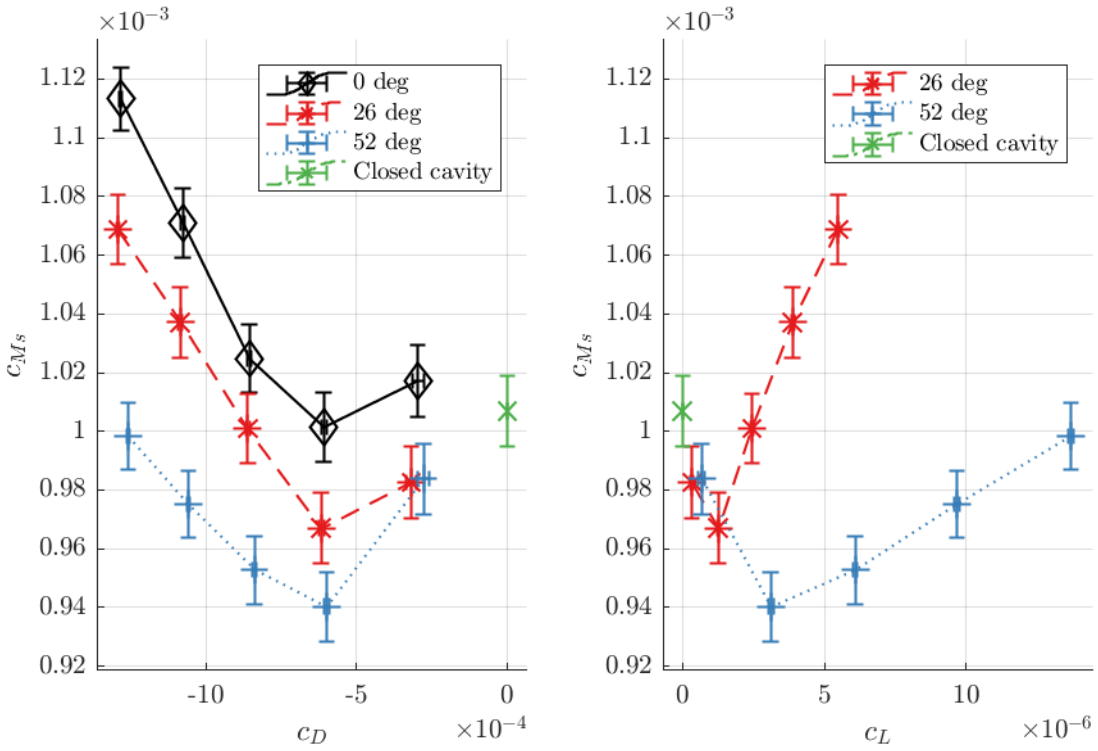

Figure 5: Torque coefficient c_{Ms} for relative gap width $G = 0.0125$ and Reynolds number $7.5 \cdot 10^7 \leq Re \leq 9.6 \cdot 10^7$ of closed cavity as well as three different preswirl angles.

It is again apparent that the flow models by Kurokawa and Sakuma (1988) fail to capture the variation of axial thrust with Reynolds number, but the influence of different cavity widths is reproduced qualitatively. Measurements published by Radtke and Ziemann (1982) are much closer to predictions by Kurokawa and Sakuma (1988) then to results from small and large test rig, and do not show any significant influence of cavity width.

CENTRIPETAL THROUGH-FLOW

In a radial turbomachine, superposed centripetal through-flow can occur in a side chamber, significantly influencing the coefficients investigated earlier. Mass flow through the cavity is given by c_D, with $c_D < 0$ for centripetal through-flow. A significant amount of angular momentum can be carried into the rotor-stator cavity if the inflow has a circumferential velocity component, this angular momentum flow is given by the coefficient c_L with $c_L > 0$ for corotational through-flow.

It is important to note that CFD simulations as well as measurements in the small test rig not presented here show a significant influence of the centripetal inlet area on the results: A jet develops at the centripetal inlet, with smaller inlet areas generating higher velocity jets for the same mass flow rate. For the large test rig, the centripetal inlet gap width d is $3.75 \cdot 10^{-3}$ times the disc radius b, while for the small test rig the relative inlet gap width is $1.82 \cdot 10^{-2}$. For this reason, results of both test rigs are presented separately.

Large test rig

The large test rig is operated in four different configurations: In addition to the closed cavity, three different preswirl guide vanes are installed, with preswirl angles $\alpha = 0°$, 26° and 52°. When $\alpha = 0$, radial inflow occurs and no angular momentum flows into the cavity, therefore $c_L = 0$. Corotational swirl corresponds to $\alpha > 0$, with angular momentum coefficient $c_L > 0$.

For a relative gap width $G = 0.0125$ and Reynolds number $7.5 \cdot 10^7 \leq Re \leq 9.6 \cdot 10^7$, the results of torque coefficient c_{Ms} with and without centripetal through-flow are displayed in Figure 5. It is apparent that with increasing centripetal mass flux, the torque coefficient c_{Ms} first decreases, reaches a minimum and then increases to higher values than the one of the closed cavity configuration.

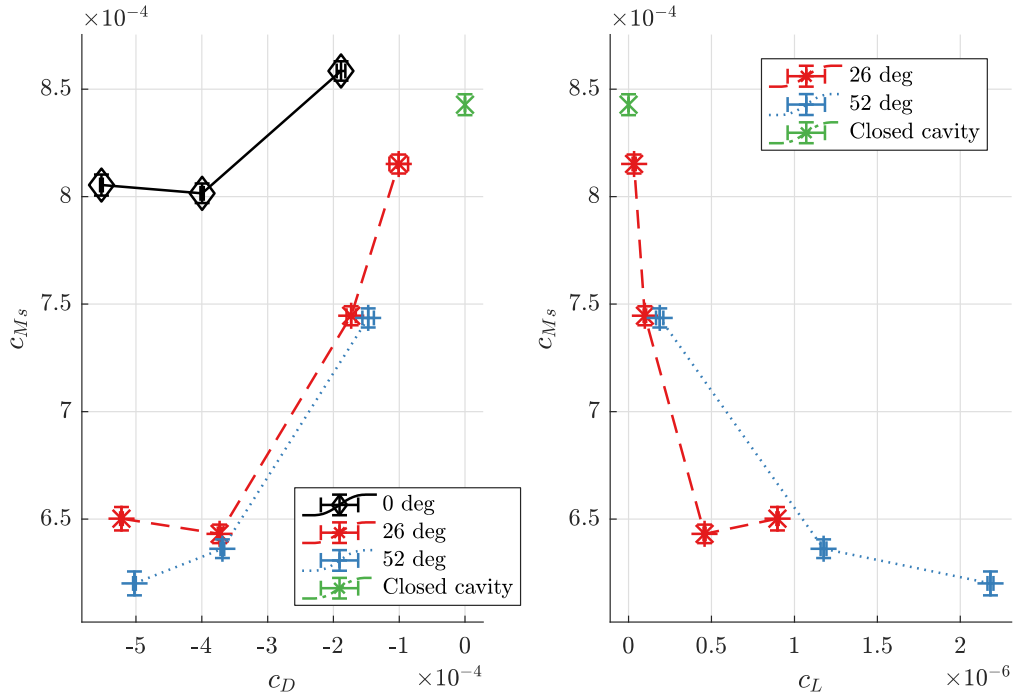

Figure 6: Torque coefficient c_{Ms} for relative gap width $G = 0.0125$ and Reynolds number $1.8 \cdot 10^8 \leq Re \leq 2.9 \cdot 10^8$ of closed cavity as well as three different preswirl angles.

Torque coefficient minima are all found at through-flow mass flux coefficients $c_D \approx -6.1 \cdot 10^{-4}$, but different angular momentum flow coefficients c_L, indicating that the point where the minima occur depends only on mass flow but not on inlet swirl angle. However, torque coefficient values strongly depend on angular momentum flow into the cavity, with high preswirl angles α leading to lower torque coefficients for constant mass flux coefficient c_D.

For large Reynolds numbers $Re \geq 1.8 \cdot 10^8$, as can be seen in Figure 6, decline of torque coefficients from radial inflow to a preswirl angle of 26° is much larger than for moderate Reynolds numbers shown in Figure 5, but torque coefficients at preswirl angles 26° and 52° differ significantly only at high through-flow mass flux (low c_D). Minimum torque coefficients are found at $c_D \approx -3.7 \cdot 10^{-4}$ for radial inflow and 26° preswirl angle, while the minimum is at $c_D \leq -5 \cdot 10^{-4}$ for 52° preswirl angle. For this gap width and Reynolds number range, angular momentum flux entering the cavity plays an important role: For radial inflow, where by definition $c_L = 0$, minimum torque coefficient is $c_{Ms} = 8 \cdot 10^{-4}$, but with increasing angular momentum inflow in the case of preswirl, torque coefficients c_{Ms} drop quickly to values below $c_{Ms} = 6.5 \cdot 10^{-4}$.

With relative cavity width $G = 0.0375$ and Reynolds number $7.5 \cdot 10^7 \leq Re \leq 9.6 \cdot 10^7$, the torque coefficient behaves as shown in Figure 8. The only difference to the measurements shown in Figure 5 is a three times larger cavity width. Again, torque coefficients are significantly higher with radial inflow (0°, no preswirl) than with preswirl, but there is no significant change between 26° and 52° preswirl angle, while such a change is observed for the small cavity width $G = 0.0125$. For this larger cavity width, minima of torque coefficient seem to be shifted to smaller through-flow mass flux coefficients c_D compared to the small cavity width, but this conclusion is not certain since the uncertainties of measured torque coefficient c_{Ms} are about as large as the change in torque coefficient itself.

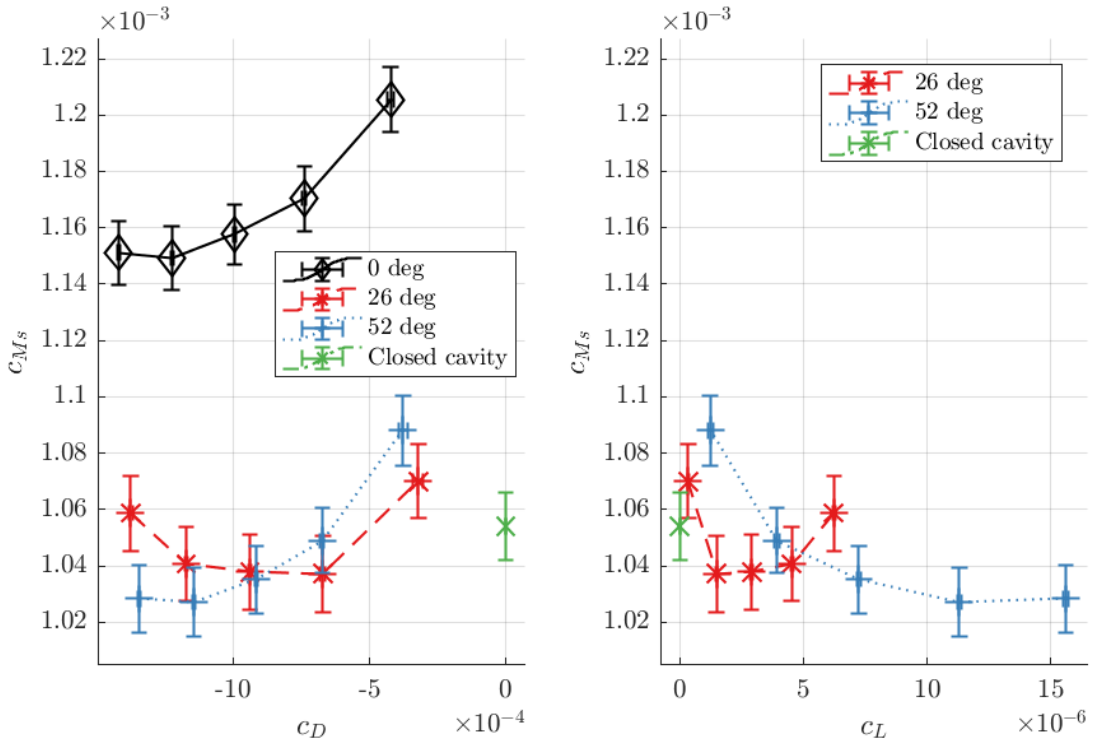

Figure 8: Torque coefficient c_{Ms} for relative gap width $G = 0.0375$ and Reynolds number $7.5 \cdot 10^7 \leq Re \leq 9.6 \cdot 10^7$ of closed cavity as well as three different preswirl angles.

Through-flow entering the cavity radially, i.e. with preswirl angle of 0°, creates a large velocity gradient in circumferential direction between fluid and disc close to the outer disc radius. This gives rise to a large drag, resulting in torque coefficients significantly higher than in cases of closed cavity or centripetal through-flow with corotating preswirl. With corotating preswirl, the difference in

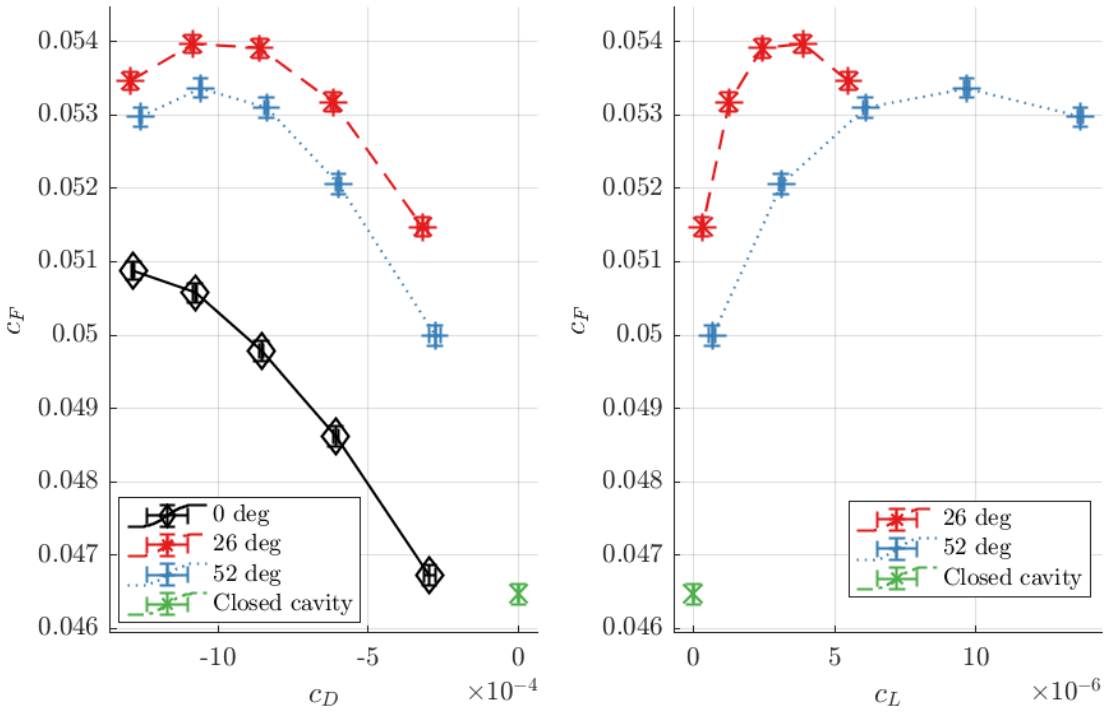

Figure 7: Axial thrust coefficient c_F for relative gap width $G = 0.0125$ and Reynolds number $7.5 \cdot 10^7 \leq Re \leq 9.6 \cdot 10^7$ of closed cavity as well as three different preswirl angles.

circumferential velocity between inflow and disc is smaller, therefore velocity gradient, drag and torque coefficient decrease.

The development of axial thrust coefficient c_F with centripetal through-flow is shown in Figure 7 for the same measurements that are shown in Figure 5 ($G = 0.0125$, $7.5 \cdot 10^7 \leq Re \leq 9.6 \cdot 10^7$): Centripetal through-flow significantly increases the thrust coefficient c_F, since centripetal through-flow is essentially an accelerated flow which results in a larger radial pressure gradient. With increasing centripetal mass flow (decreasing c_D), the axial thrust coefficient c_F reaches a maximum for preswirl angles 26° and 52° at $c_D \approx -1.1 \cdot 10^{-3}$. For radial inflow, it seems that the thrust coefficient c_F converges towards a maximum, too, which is outside of the investigated through-flow mass flux rate. For this gap width and Reynolds number, centripetal through-flow with preswirl angles of 26° and 52° generates higher axial thrust coefficients compared to radial inflow with a preswirl angle of 0°. The small difference in axial thrust coefficient between measurements with 26° and 52° preswirl angle is not considered significant, because it might stem from a slightly higher Reynolds number of the measurements with 52° preswirl angle. The angular momentum coefficient c_L alone is again insufficient to describe the axial thrust because for one angular momentum coefficient value, multiple different axial thrust coefficient values are observed.

To investigate the influence of mass flow and angular momentum on axial thrust coefficients, radial pressure distribution of the closed cavity as well as centripetal through-flow with 52° preswirl angle is plotted in Figure 9. No markers or error bars are shown for easier view of the pressure gradients. With increasing centripetal through-flow, pressure at radii $x < 0.7$ decreases, as indicated by larger pressure coefficient values c_p. Simultaneously, pressure at radii $0.75 < x < 1$ increases, leading to lower pressure coefficients c_p compared to the closed cavity. Since in the computation of axial thrust coefficient c_F pressure coefficients c_p are weighted with relative radial position x, a small pressure increase at large relative radii x can balance larger pressure drops at small radii x. This happens at maxima of thrust coefficients c_F, where a change in radial pressure distribution does not cause a change in axial thrust coefficient c_F.

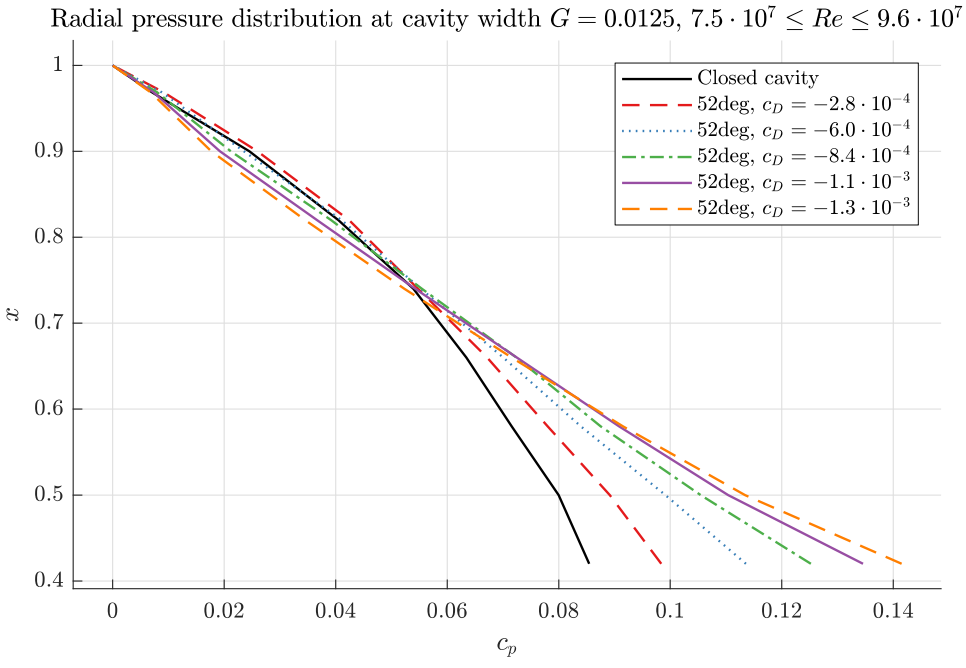

Figure 9: Radial pressure distribution at relative cavity width $G = 0.0125$, Reynolds numbers $7.5 \cdot 10^7 \leq Re \leq 9.6 \cdot 10^7$, closed cavity and 52° preswirl angle with centripetal through-flow.

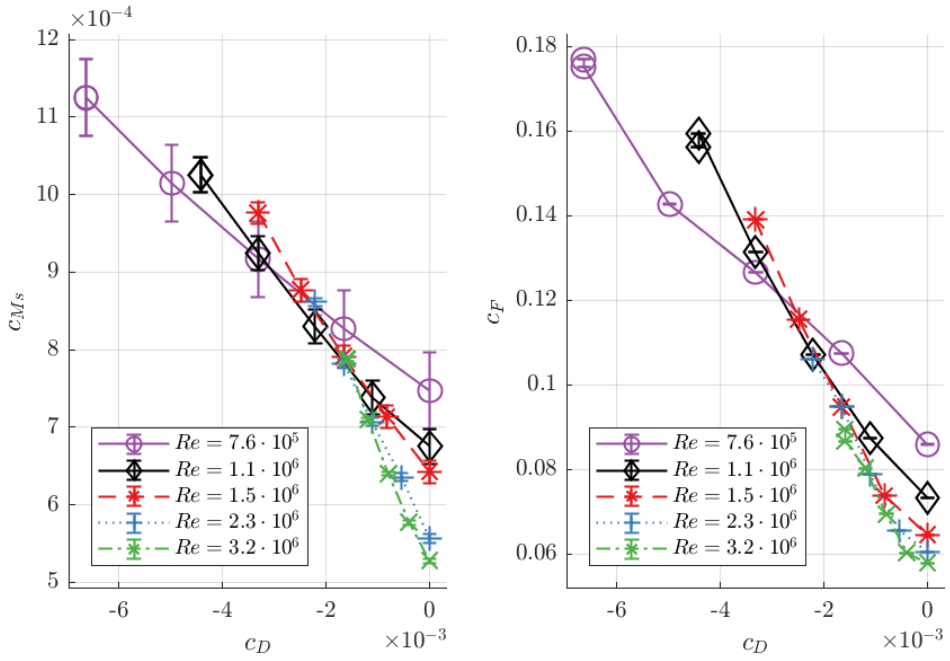

Figure 10: Axial thrust coefficient c_F and torque coefficient c_{Ms} measured in the small test rig (compare Hu (2018)) with closed cavity ($c_D = 0$) and radial inflow ($\alpha = 0$, $c_D < 0$) for the small relative cavity width $G = 0.0182$.

Small test rig

Axial thrust coefficients c_F and torque coefficients c_{Ms} measured in the small test rig with closed cavity as well as radial inflow are shown in Figure 10. The figure shows data from the small relative cavity width $G = 0.0182$. The results show an almost linear increase of thrust and torque coefficients with decreasing through-flow coefficient c_D, with the slope depending on circumferential Reynolds number Re: With increasing Reynolds number Re, the slopes $\partial c_{Ms}/\partial c_D$ and $\partial c_F/\partial c_D$ decrease.

In comparison with results from the large test rig, it appears that the torque coefficient minimum, which is observed in the large test rig for moderate through-flow mass flow rates and radial inflow, does not appear in the measurements in the small test rig. The axial thrust coefficient c_F of the large test rig with radial inflow, which is plotted in Figure 7, increases with decreasing through-flow coefficient c_D, just like in the small test rig. But in the large test rig, this increase decelerates with decreasing through-flow coefficient c_D, while in the small test rig, this deceleration is not apparent.

In Figure 11, the influence of preswirl angle on torque and axial thrust coefficients for the small test rig is presented. It is important to note that in this figure, Reynolds number of a data point is found on the upper horizontal axis while the through-flow coefficient is found on the lower one. Torque coefficient behaviour with varying preswirl angle is similar to the behaviour observed in the large test rig: With preswirl angle increasing from 0° (radial inflow) to 26°, torque coefficient drops sharply, while a further increase of preswirl angle to 52° only leads to a marginal decrease of torque coefficient compared to the results with 26° preswirl angle. Regarding thrust coefficients, it is found that an increase in preswirl angle increases thrust coefficient c_F, just like in the large test rig. Interestingly, this increase is very small at the operating point $Re \approx 2 \cdot 10^6$, $c_D \approx -3 \cdot 10^{-3}$, but larger at all other points.

CONCLUSIONS

For the closed cavity, decrease of torque coefficient c_{Ms} with increasing Reynolds number behaves in the same way as found experimentally by Daily and Nece (1960) and as predicted by Kurokawa and Toyokura (1972) for Reynolds numbers $Re \leq 3.2 \cdot 10^6$. For larger Reynolds numbers,

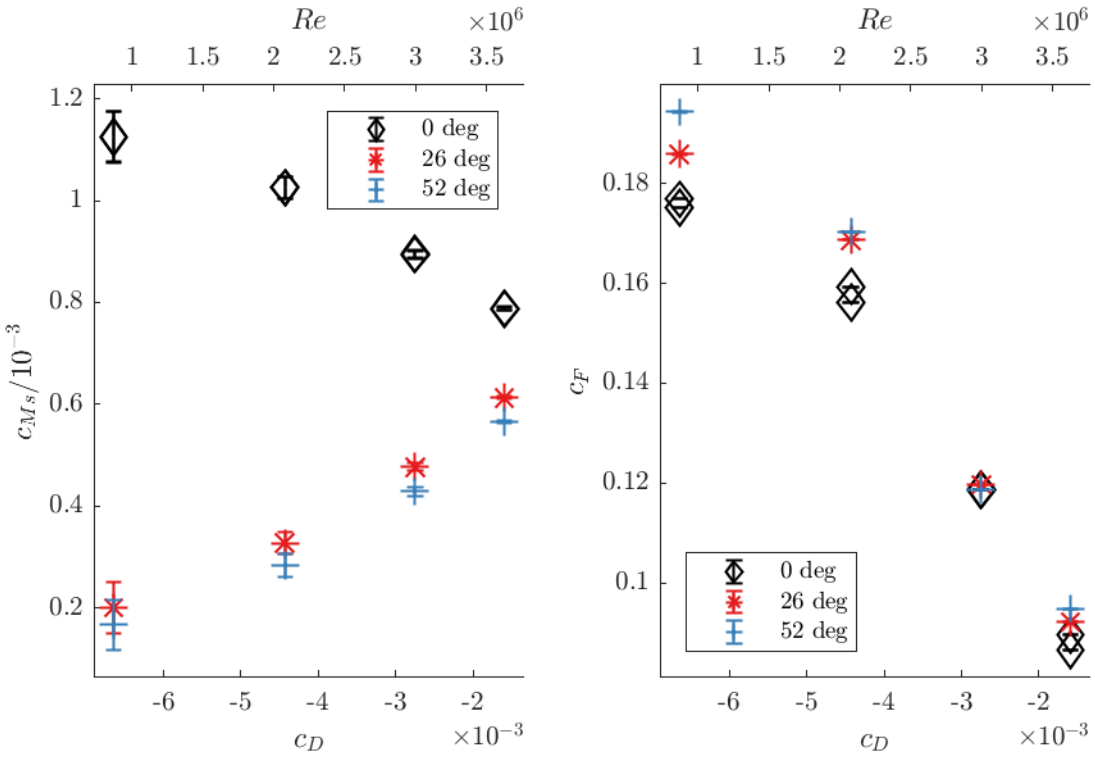

Figure 11: Influence of preswirl angle on torque and moment coefficient in the small test rig (compare Hu (2018)) with relative cavity width $G = 0.0182$. For the results shown here, the product $c_D \cdot Re$ is constant.

torque coefficient c_{Ms} decreases significantly slower with increasing Reynolds numbers. This behaviour is observed in two different test rigs with two different fluids (Carbon dioxide and air).

Both models introduced by Kurokawa and Sakuma (1988) fail to correctly predict the influence of Reynolds number Re on radial pressure distribution and axial thrust coefficient c_F, but capture the influence of relative axial gap width G qualitatively: With increasing Reynolds number, axial thrust coefficient decreases; with increasing cavity width, axial thrust coefficient increases.

In the large test rig with centripetal through-flow, torque coefficients c_{Ms} first decrease with decreasing mass flow coefficient c_D compared to the closed cavity configuration, reach a minimum and start to increase with further decrease of mass flow coefficient c_D. The torque coefficient minimum is found at different mass flow coefficients c_D, depending on Reynolds number Re, relative axial gap width G, and preswirl angle α. This minimum is not found in the small, water-operated test rig, where centripetal through-flow with radial inflow increases torque coefficients c_{Ms}.

Increasing preswirl angle α from $\alpha = 0°$ to $\alpha = 26°$ leads to a reduction in torque coefficient c_{Ms} in the large and in the small test rig, however, only at Reynolds numbers $7.5 \cdot 10^7 \leq Re \leq 9.6 \cdot 10^7$ and small cavity width $G = 0.0125$ a further reduction of torque coefficient c_{Ms} is observed in the large test rig when preswirl angle is increased to $52°$. All other measurements presented here do not show significant differences between preswirl angles of $26°$ and $52°$.

For a small gap width $G = 0.0125$ and Reynolds number range $7.5 \cdot 10^7 \leq Re \leq 9.6 \cdot 10^7$, mass flow coefficients $c_D < 0$ with any preswirl angles investigated lead to larger axial thrust coefficients c_F compared to a closed cavity. A characteristic maximum of axial thrust coefficients is observed for preswirl angles $26°$ and $52°$. For radial inflow, the coefficients seem to converge towards a maximum, which is outside the test rig's operating range. Almost the same behaviour of axial thrust coefficient is observed in the small test rig with radial inflow, where centripetal through-flow increases axial thrust coefficient, but no signs of maxima are found. Concerning the influence of preswirl angle, it is found that an increase in preswirl angle results in an increase in axial thrust coefficient both in the large as well as in the small test rig.

The increase of axial thrust coefficients with centripetal through-flow and 52° preswirl angle observed in the large test rig are a result of pressure increasing at relative radii $x > 0.75$ and decreasing at relative radii $x < 0.7$ compared to a closed cavity radial pressure distribution.

ACKNOWLEDGEMENTS

The research conducted with the large test rig is funded jointly by BMWi (Bundesministerium für Wirtschaft und Technologie of the German government) and Siemens Power and Gas, Compressors. The authors are grateful for the financial support under contract number 03ET7071C.

REFERENCES

Barabas, B., Clauss, S., Schuster, S., Benra, F.-K., Dohmen, H.-J., Brillert, D. (2015). *Experimental and numerical determination of pressure and velocity distribution inside a rotor-stator cavity at very high circumferential Reynolds numbers.* Proceedings of the 11th European Conference on Turbomachinery.

Bevington, P. R., Robinson, D. K. (2003). *Data Reduction and Error Analysis for the Physical Sciences. Third Edition.* McGraw Hill, New York, United States of America.

Daily, J. W., Nece, R. E., (1960). *Chamber Dimension Effects on Induced Flow and Frictional Resistance of Enclosed Rotating Disks.* Journal of Basic Engineering 82 (1)

Hu, B., (2018). *Numerical and Experimental Investigation on the Flow in Rotor-Stator Cavities.* Dissertation, Chair of Turbomachinery, University of Duisburg-Essen, Germany.

Hu, B., Brillert, D., Dohmen, H.-J., Benra, F.-K., (2017). *Investigation on the flow in a rotor-stator cavity with centripetal through-flow.* Proceedings of 12th European Conference on Turbomachinery, Stockholm, Sweden

Hu, B., Brillert, D., Dohmen, H.-J., Benra, F.-K., (2017). *Investigation on the Influence of Surface Roughness on the Moment Coefficient in a Rotor-Stator Cavity with Centripetal Through-Flow.* Proceedings of the ASME 2017, Waikoloa, USA.

Kurokawa, J., Toyokura, T. (1972). *Study on Axial Thrust of Radial Flow Turbomachinery.* Proceedings of the Second International JSME Symposium Fluid Machinery and Fluidics, Tokyo

Kurokawa, J., Sakuma, M., (1988). *Flow in a Narrow Gap Along an Enclosed Rotating Disk with Through-Flow.* JSME international journal Series 2, Volume 31, No. 2

Poncet, S., Chauve, M. P., Le Gal, P., (2005). *Turbulent rotating disk flow with inward throughflow.* Journal of Fluid Mechanics, Volume 522.

Poncet, S., Chauve, M.-P., Schiestel, R., (2005). *Batchelor versus Stewartson flow structures in a rotor-stator cavity with throughflow.* Physics of Fluids (17), 2005.

Radtke, F., Ziemann, M., (1982). *Scheibenreibung: Experimentelle und theoretische Untersuchungen des Reibungseinflusses an rotierenden Scheiben.* FVV-Bericht Nr. 213

Wang, C., Tang, F., Li, Q., Wang, X., (2018). *Experimental investigation of the microscale rotor-stator cavity flow with rotating superhydrophobic surface.* Experiments in Fluids (2018) 59: 47.

Weise, K., Wöger, W., (1999). *Meßunsicherheit und Meßdatenauswertung.* Wiley-VCH

Will, B.-C., (2011). *Theoretical, Numerical and Experimental Investigation of the Flow in Rotor-Stator Cavities with Application to a Centrifugal Pump*. Dissertation, Chair of Turbomachinery, University of Duisburg-Essen, Germany.